Editors' Suggestion

Observation of Complex Time Structures in the Cosmic-Ray Electron and Positron Fluxes with the Alpha Magnetic Spectrometer on the International Space Station

M. Aguilar,[27] L. Ali Cavasonza,[1] G. Ambrosi,[32] L. Arruda,[25] N. Attig,[22] S. Aupetit,[18] P. Azzarello,[17] A. Bachlechner,[1] F. Barao,[25] A. Barrau,[18] L. Barrin,[16] A. Bartoloni,[37] L. Basara,[35] S. Başeğmez-du Pree,[6] M. Battarbee,[45] R. Battiston,[35,36,a] U. Becker,[10] M. Behlmann,[10] B. Beischer,[1] J. Berdugo,[27] B. Bertucci,[32,33] K. F. Bindel,[23] V. Bindi,[20] W. de Boer,[23] K. Bollweg,[21] V. Bonnivard,[18] B. Borgia,[37,38] M. J. Boschini,[29] M. Bourquin,[17] E. F. Bueno,[39] J. Burger,[10] F. Cadoux,[17] X. D. Cai,[10] M. Capell,[10] S. Caroff,[3] J. Casaus,[27] G. Castellini,[15] F. Cervelli,[34] M. J. Chae,[40] Y. H. Chang,[11] A. I. Chen,[10] G. M. Chen,[6] H. S. Chen,[6,7] Y. Chen,[17] L. Cheng,[41] H. Y. Chou,[11] E. Choumilov,[10] V. Choutko,[10] C. H. Chung,[1] C. Clark,[21] R. Clavero,[24] G. Coignet,[3] C. Consolandi,[20] A. Contin,[8,9] C. Corti,[20] W. Creus,[44] M. Crispoltoni,[32,33] Z. Cui,[41] K. Dadzie,[10] Y. M. Dai,[5] A. Datta,[20] C. Delgado,[27] S. Della Torre,[29] M. B. Demirköz,[2] L. Derome,[18] S. Di Falco,[34] F. Dimiccoli,[35,36] C. Díaz,[27] P. von Doetinchem,[20] F. Dong,[31] F. Donnini,[32,33] M. Duranti,[32] D. D'Urso,[32,b] A. Egorov,[10] A. Eline,[10] T. Eronen,[45] J. Feng,[10] E. Fiandrini,[32,33] P. Fisher,[10] V. Formato,[32] Y. Galaktionov,[10] G. Gallucci,[34] R. J. García-López,[24] C. Gargiulo,[16] H. Gast,[1] I. Gebauer,[23] M. Gervasi,[29,30] A. Ghelfi,[18] F. Giovacchini,[27] D. M. Gómez-Coral,[28] J. Gong,[31] C. Goy,[3] V. Grabski,[28] D. Grandi,[29] M. Graziani,[23] K. H. Guo,[19] S. Haino,[44] K. C. Han,[26] Z. H. He,[19] M. Heil,[10] T. H. Hsieh,[10] H. Huang,[44,c] Z. C. Huang,[19] C. Huh,[14] M. Incagli,[34] M. Ionica,[32] W. Y. Jang,[14] Yi Jia,[10] H. Jinchi,[26] S. C. Kang,[14] K. Kanishev,[35,16] B. Khiali,[11] G. N. Kim,[14] K. S. Kim,[14] Th. Kirn,[1] C. Konak,[2] O. Kounina,[10] A. Kounine,[10] V. Koutsenko,[10] A. Kulemzin,[10] G. La Vacca,[29,30] E. Laudi,[16] G. Laurenti,[8] I. Lazzizzera,[35,36] A. Lebedev,[10] H. T. Lee,[43] S. C. Lee,[44] C. Leluc,[17] H. S. Li,[42] J. Q. Li,[31] Q. Li,[31] T. X. Li,[19] Z. H. Li,[6] Z. Y. Li,[44,d] S. Lim,[14] C. H. Lin,[44] P. Lipari,[37] T. Lippert,[22] D. Liu,[11] Hu Liu,[10] V. D. Lordello,[39] S. Q. Lu,[44,d] Y. S. Lu,[6] K. Luebelsmeyer,[1] F. Luo,[41] J. Z. Luo,[31] S. S. Lyu,[19] F. Machate,[1] C. Mañá,[27] J. Marín,[27] T. Martin,[21] G. Martínez,[27] N. Masi,[8] D. Maurin,[18] A. Menchaca-Rocha,[28] Q. Meng,[31] V. M. Mikuni,[39] D. C. Mo,[19] P. Mott,[21] T. Nelson,[20] J. Q. Ni,[19] N. Nikonov,[1] F. Nozzoli,[32,35,e] A. Oliva,[27] M. Orcinha,[25] M. Palermo,[20] F. Palmonari,[8,9] C. Palomares,[27] M. Paniccia,[17] M. Pauluzzi,[32,33] S. Pensotti,[29,30] C. Perrina,[17] H. D. Phan,[10] N. Picot-Clemente,[13] F. Pilo,[34] C. Pizzolotto,[32,f] V. Plyaskin,[10] M. Pohl,[17] V. Poireau,[3] L. Quadrani,[8,9] X. M. Qi,[19] X. Qin,[10] Z. Y. Qu,[44,g] T. Räihä,[1] P. G. Rancoita,[29] D. Rapin,[17] J. S. Ricol,[18] S. Rosier-Lees,[3] A. Rozhkov,[10] D. Rozza,[29,30] R. Sagdeev,[12] S. Schael,[1] S. M. Schmidt,[22] A. Schulz von Dratzig,[1] G. Schwering,[1] E. S. Seo,[13] B. S. Shan,[4] J. Y. Shi,[31] T. Siedenburg,[1] D. Son,[14] J. W. Song,[41] M. Tacconi,[29,30] X. W. Tang,[6] Z. C. Tang,[6] D. Tescaro,[24] Samuel C. C. Ting,[10,16] S. M. Ting,[10] N. Tomassetti,[32,33] J. Torsti,[45] C. Türkoğlu,[2] T. Urban,[21] V. Vagelli,[32,33] E. Valente,[37,38] E. Valtonen,[45] M. Vázquez Acosta,[24] M. Vecchi,[39] M. Velasco,[27] J. P. Vialle,[3] L. Q. Wang,[41] N. H. Wang,[41] Q. L. Wang,[5] X. Wang,[10] X. Q. Wang,[6,7] Z. X. Wang,[19] C. C. Wei,[44,h] Z. L. Weng,[10] K. Whitman,[20] H. Wu,[31] X. Wu,[17] R. Q. Xiong,[31] W. Xu,[10] Q. Yan,[10] J. Yang,[40] M. Yang,[6] Y. Yang,[42] H. Yi,[31] Y. J. Yu,[5] Z. Q. Yu,[6] M. Zannoni,[29,30] S. Zeissler,[23] C. Zhang,[6] F. Zhang,[6] J. Zhang,[10] J. H. Zhang,[31] S. W. Zhang,[6,7] Z. Zhang,[10] Z. M. Zheng,[4] H. L. Zhuang,[6] V. Zhukov,[1] A. Zichichi,[8,9] N. Zimmermann,[1] and P. Zuccon[10]

(AMS Collaboration)

[1]*I. Physics Institute and JARA-FAME, RWTH Aachen University, D–52056 Aachen, Germany*
[2]*Department of Physics, Middle East Technical University (METU), 06800 Ankara, Turkey*
[3]*Laboratoire d'Annecy–le–Vieux de Physique des Particules (LAPP), CNRS/IN2P3 and Université Savoie Mont Blanc, F–74941 Annecy–le–Vieux, France*
[4]*Beihang University (BUAA), Beijing, 100191, China*
[5]*Institute of Electrical Engineering (IEE), Chinese Academy of Sciences, Beijing, 100190, China*
[6]*Institute of High Energy Physics (IHEP), Chinese Academy of Sciences, Beijing, 100049, China*
[7]*University of Chinese Academy of Sciences (UCAS), Beijing, 100049, China*
[8]*INFN Sezione di Bologna, I–40126 Bologna, Italy*
[9]*Università di Bologna, I–40126 Bologna, Italy*
[10]*Massachusetts Institute of Technology (MIT), Cambridge, Massachusetts 02139, USA*
[11]*National Central University (NCU), Chung–Li, Tao Yuan, 32054, Taiwan*
[12]*East–West Center for Space Science, University of Maryland, College Park, Maryland 20742, USA*
[13]*IPST, University of Maryland, College Park, Maryland 20742, USA*
[14]*CHEP, Kyungpook National University, 41566 Daegu, Korea*
[15]*CNR–IROE, I-50125 Firenze, Italy*

[16]European Organization for Nuclear Research (CERN), CH–1211 Geneva 23, Switzerland

[17]DPNC, Université de Genève, CH–1211 Genève 4, Switzerland

[18]Laboratoire de Physique Subatomique et de Cosmologie (LPSC), CNRS/IN2P3 and Université Grenoble–Alpes, F–38026 Grenoble, France

[19]Sun Yat–Sen University (SYSU), Guangzhou, 510275, China

[20]Physics and Astronomy Department, University of Hawaii, Honolulu, Hawaii 96822, USA

[21]National Aeronautics and Space Administration Johnson Space Center (JSC), Jacobs Engineering, and Business Integra, Houston, Texas 77058, USA

[22]Jülich Supercomputing Centre and JARA-FAME, Research Centre Jülich, D–52425 Jülich, Germany

[23]Institut für Experimentelle Teilchenphysik, Karlsruhe Institute of Technology (KIT), D–76131 Karlsruhe, Germany

[24]Instituto de Astrofísica de Canarias (IAC), E–38205 La Laguna, and Departamento de Astrofísica, Universidad de La Laguna, E–38206 La Laguna, Tenerife, Spain

[25]Laboratório de Instrumentação e Física Experimental de Partículas (LIP), P–1000 Lisboa, Portugal

[26]National Chung–Shan Institute of Science and Technology (NCSIST), Longtan, Tao Yuan, 32546, Taiwan

[27]Centro de Investigaciones Energéticas, Medioambientales y Tecnológicas (CIEMAT), E–28040 Madrid, Spain

[28]Instituto de Física, Universidad Nacional Autónoma de México (UNAM), México, D. F., 01000 Mexico

[29]INFN Sezione di Milano–Bicocca, I–20126 Milano, Italy

[30]Università di Milano–Bicocca, I–20126 Milano, Italy

[31]Southeast University (SEU), Nanjing, 210096, China

[32]INFN Sezione di Perugia, I–06100 Perugia, Italy

[33]Università di Perugia, I–06100 Perugia, Italy

[34]INFN Sezione di Pisa, I–56100 Pisa, Italy

[35]INFN TIFPA, I–38123 Povo, Trento, Italy

[36]Università di Trento, I–38123 Povo, Trento, Italy

[37]INFN Sezione di Roma 1, I–00185 Roma, Italy

[38]Università di Roma La Sapienza, I–00185 Roma, Italy

[39]Instituto de Física de São Carlos, Universidade de São Paulo, CP 369, 13560-970, São Carlos, São Paulo, SP, Brazil

[40]Department of Physics, Ewha Womans University, Seoul, 120-750, Korea

[41]Shandong University (SDU), Jinan, Shandong, 250100, China

[42]National Cheng Kung University, Tainan, 70101, Taiwan

[43]Academia Sinica Grid Center (ASGC), Nankang, Taipei, 11529, Taiwan

[44]Institute of Physics, Academia Sinica, Nankang, Taipei, 11529, Taiwan

[45]Space Research Laboratory, Department of Physics and Astronomy, University of Turku, FI–20014 Turku, Finland

We present high-statistics, precision measurements of the detailed time and energy dependence of the primary cosmic-ray electron flux and positron flux over 79 Bartels rotations from May 2011 to May 2017 in the energy range from 1 to 50 GeV. For the first time, the charge-sign dependent modulation during solar maximum has been investigated in detail by leptons alone. Based on 23.5×10^6 events, we report the observation of short-term structures on the timescale of months coincident in both the electron flux and the positron flux. These structures are not visible in the e^+/e^- flux ratio. The precision measurements across the solar polarity reversal show that the ratio exhibits a smooth transition over 830 ± 30 days from one value to another. The midpoint of the transition shows an energy dependent delay relative to the reversal and changes by 260 ± 30 days from 1 to 6 GeV.

In this Letter, we present precision measurements of the primary cosmic-ray electron flux, positron flux, and e^+/e^- flux ratio R_e in the energy range from 1 to 50 GeV as a function of Bartels rotation (27 days), from May 2011 to May 2017, based on 23.5×10^6 electron and positron events collected by the Alpha Magnetic Spectrometer (AMS) aboard the International Space Station (ISS). These data allow comprehensive studies of the energy and charge-sign dependence of short-term effects on the time scale of months, related to solar activity [1,2], and long-term effects on the time scale of years, related to the 22 year cycle of the solar magnetic field [3].

The fluxes of interstellar charged cosmic rays are thought to be stable on the time scale of decades [4–7].

Time-dependent structures in the energy spectra are only expected from the solar modulation [3] of interstellar cosmic rays when they enter the heliosphere. Solar modulation involves convective, diffusive, particle drift, and adiabatic energy loss processes. Only particle drift induces a dependence of solar modulation on the particle charge sign [8]. Since electrons and positrons differ only in charge sign, their simultaneous measurement offers a unique way to study charge-sign dependent solar modulation effects. Previous experiments have established that solar modulation is charge-sign dependent [9–12]. The important difference to earlier studies [10,13–16] is the high statistics of the data presented in this Letter which allow for the first time precision measurements with a time resolution of one month for particles with identical mass but opposite charge sign. This measurement will continue for the entire solar cycle (∼2024) and provide a comparison to earlier measurements [16]. Our data were collected continuously during the polarity reversal of the solar magnetic field, which took place in the year 2013 [17], at the time of the solar maximum in solar cycle 24. Therefore one expects large charge-sign dependent effects on R_e.

In addition to the long-term variations of cosmic-ray fluxes related to the solar cycle, short-term structures in the cosmic-ray proton flux [1,18] and helium flux [18] have been observed, which could occasionally be related to particular events in the solar activity. With the precision data on electrons and positrons measured simultaneously over an extended period of time, we are able to measure the difference in time-dependent structures in the fluxes of particles and antiparticles from solar effects for the first time.

The time structure of particle to antiparticle ratios like R_e is of particular importance as these ratios have been widely used to search for new phenomena in primary cosmic rays such as the existence of a nearby positron source [19] or dark matter annihilation [20,21]. Model predictions can only be compared properly to data from long-duration experiments or experiments at different times when short-term effects caused by the activity of the Sun and long-term effects that impact solar modulation are taken into account. Our precise data on the time and energy dependence of the electron flux and positron flux at 1 AU provide new and additional accurate input and detailed constraints on modeling of the transport processes for charged cosmic rays inside the heliosphere [22–25]. A comprehensive model of the time-dependent solar modulation will have far-reaching consequences for the understanding of currently unexplained features in cosmic-ray fluxes, such as the observed rise of the positron fraction above 8 GeV [26], as well as for other domains of astrophysics, such as the modeling of galactic cosmic-ray propagation [27], the estimate of the galactic cosmic-ray pressure, an important ingredient for models of galaxy formation [28], and the interpretation of possible anisotropies in the cosmic-ray arrival directions at Earth [29].

Detector.—The AMS-02 detector consists of a permanent magnet, nine planes of silicon tracker, a transition radiation detector (TRD), four planes of time-of-flight counters, an array of 16 anticoincidence counters, a ring imaging Čerenkov detector (RICH), and an electromagnetic calorimeter (ECAL). The AMS operates continuously on the ISS and is monitored and controlled continuously from the ground. A detailed description of the instrument is found in Ref. [30]. Monte Carlo simulated events were produced using a dedicated program developed by the collaboration based on the GEANT-4.10.1 package [31]. The program simulates electromagnetic and hadronic interactions of particles in the material of the AMS and generates detector responses. The Monte Carlo event samples have sufficient statistics such that they do not contribute to the errors.

Data analysis.—The data analysis follows the procedure used for our measurement of the time-averaged electron and positron fluxes [32] with improved low-energy effective acceptance [33]. The fluxes of cosmic-ray positrons and electrons for Bartels rotation i in the energy bin E of width ΔE are given by

$$\Phi_{e^\pm,i}(E) = \frac{N_{e^\pm,i}(E)}{A_{\text{eff},i}(E)T_i(E)\epsilon_{\text{trig}}(E)\Delta E}, \quad (1)$$

where $N_{e^+,i}$ and $N_{e^-,i}$ are the numbers of positrons and electrons, respectively, $A_{\text{eff},i}$ is the effective acceptance, and T_i is the exposure time in the given time bin. ϵ_{trig} is the trigger efficiency, which is found to be stable over time, and is 100% above 3 GeV decreasing to 75% at 1 GeV. The same energy binning as for Ref. [32] is used up to 49.33 GeV.

The effective acceptance is defined as

$$A_{\text{eff},i}(E) = A_{\text{geom}}\epsilon(E)[1 + \delta(E)](1 + \hat{\delta}_i), \quad (2)$$

where $A_{\text{geom}} = 550 \text{ cm}^2$ sr is the geometric acceptance, ϵ is the selection and identification efficiency, and the product $A_{\text{geom}}\epsilon$ is determined by Monte Carlo simulation. The time-independent function $\delta(E)$ corrects for minor differences between simulation and data and is determined in the same way as in Ref. [32]. The absolute value of $\delta(E)$ was found to be < 4% over the entire energy range. The $\hat{\delta}_i$ account for small time-dependent effects in the detector response and vary at the level of $(0.0 \pm 0.4)\%$.

The exposure time $T_i(E)$ is determined as a function of energy for each Bartels rotation by counting the number of livetime-weighted seconds at each location above the geomagnetic cutoff [32], when the detector was in normal operating conditions and, in addition, the AMS was pointing within 40° of the local zenith and the ISS was outside of the South Atlantic Anomaly. The function $T_i(E)$ reaches a value of 80% of a Bartels rotation at energies above 35 GeV and smoothly declines towards lower

energies, due to the geomagnetic cutoff. It is 6% of a Bartels rotation at 2 GeV. Below 1 GeV, the geomagnetic cutoff does not allow us to resolve the time structure of the fluxes.

To match with the high statistics, we have performed extensive systematic studies as in Ref. [32]. These uncertainties affect all time bins in the same way. The relative systematic uncertainty on the flux is below 2.5% for both electrons and positrons for all energies. The main contribution to this small systematic error is from the uncertainty on the effective acceptance for electrons and positrons at energies below 2 GeV and from charge confusion for positrons above 2 GeV. Charge confusion occurs when an electron is reconstructed as a positron and vice versa; for details see Ref. [32]. For all Bartels rotations and for all energies, the systematic error on the positron flux is smaller than the statistical error; for the electron flux this is the case above 10 GeV.

The uncertainty on the absolute energy scale of the ECAL [32] is 4.3% at 1 GeV, decreasing to 2% in the range 10–50 GeV. This is treated as an uncertainty of the bin boundaries. The bin widths ΔE are chosen to be at least 2 times the energy resolution to minimize migration effects. With the high statistics of six years, the algorithms used to determine the energy calibration of the ECAL have been optimized compared to Refs. [26,32] leading to energy-dependent corrections $< 1.5\%$ of the energy scale.

The time stability of the energy scale is monitored using the ratio E/p of the energy measured in the ECAL E to the momentum measured in the tracker p. The momentum scale is monitored by measurements of the proton mass using the velocity measured by the RICH and the momentum measured by the tracker. The energy scale is found to be stable at the level of 0.2% for all Bartels rotations and all energies. This produces a negligible uncertainty on the fluxes and R_e.

Most importantly, several independent analyses were performed on the same data sample. The results of those analyses are consistent with the results presented in this Letter.

Results.— The results on the time-dependent primary cosmic-ray electron flux, positron flux, and their ratio R_e are provided in the Supplemental Material [34] as functions of energy at the top of the AMS. The time-averaged electron flux, positron flux, and the ratio R_e are shown in Fig. 1 and listed in Table I of the Supplemental Material [34]. In Fig. 1, the points are placed horizontally at $\tilde{E}$ calculated for a flux $\propto E^{-3}$ [35]. The event selection criteria in the analyses for the fluxes Φ_{e^+}, Φ_{e^-}, and the ratio R_e were optimized independently, see Refs. [26,32]. This accounts for the minute differences between R_e given in the tables and that calculated from Φ_{e^+}/Φ_{e^-}. The improved precision on R_e is apparent from Table I of the Supplemental Material [34].

To search for fine structures in the energy dependence of the fluxes, the model given in Ref. [36] was compared to the data for each Bartels rotation independently. The
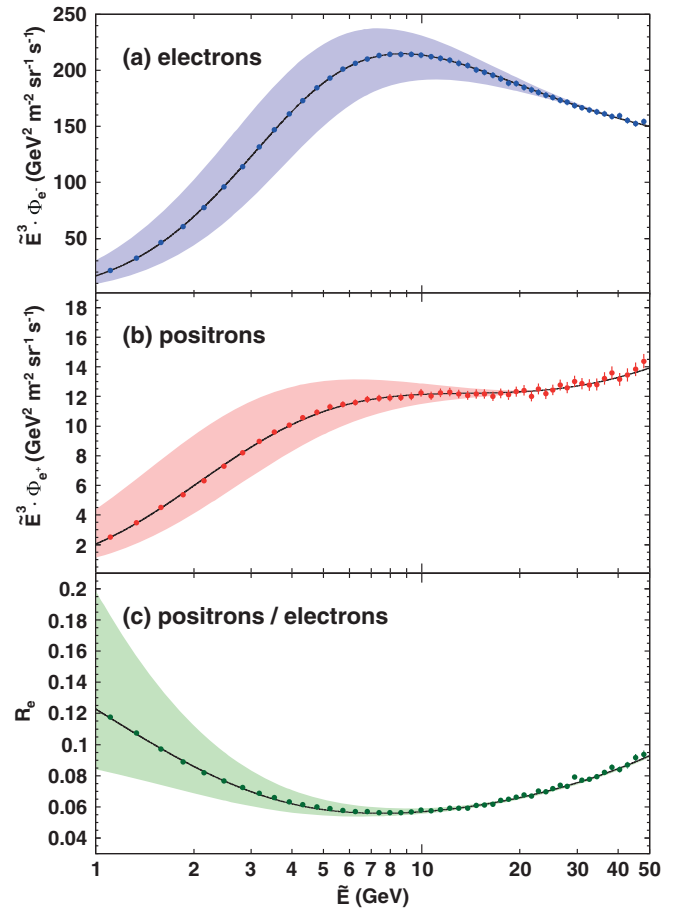

FIG. 1. The time-averaged (a) electron flux, (b) positron flux, and (c) ratio R_e. The time-variation range is indicated by the shaded regions, see text. The fit of the model in Refs. [36,37] to the time-averaged data points is shown by the black curves. The visible time variation of R_e is evidence for charge-sign dependent solar modulation.

positron data show no additional structure, see Fig. SM 1 in the Supplemental Material [34], but the electron data reveal a model dependent residual structure in the energy range between 2 and 3 GeV, see Fig. SM 2 [34], which is stable in time and consistent with an additional smooth break [37,38] in the electron spectral index $\gamma_{e^-} = d(\log \Phi_{e^-})/d(\log E)$ below 10 GeV (Fig. SM 3 [34]), comparable to the local interstellar electron spectrum of Ref. [39]. The fits of the extended model [36] to our data yield an average $\chi^2/\text{d.o.f.} \approx 1$ for all Bartels rotations and no fine structures in the energy spectra were found.

To visualize the magnitude of the time variations of the fluxes and of R_e, the envelopes of all fitted curves are displayed in Fig. 1 as shaded regions. The amplitude of the shaded regions decreases with increasing energy. At high energies, the statistical bin-to-bin fluctuations are larger than the time variation. As seen in Fig. 1(c), the clear time variation of R_e is evidence for charge-sign dependent solar modulation.
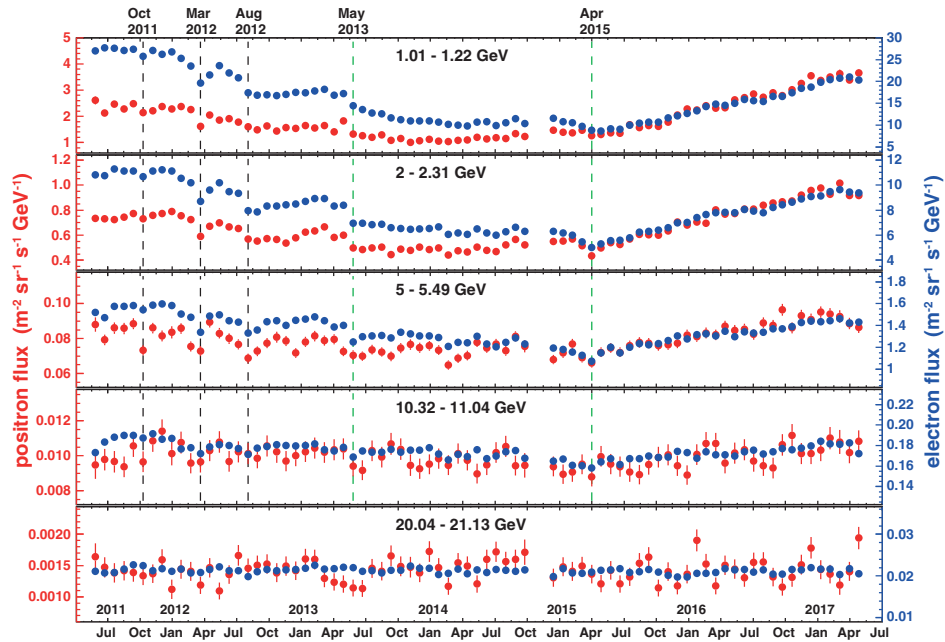
FIG. 2. Fluxes of primary cosmic-ray positrons (red, left axis) and electrons (blue, right axis) as functions of time, for five of the 49 energy bins. The error bars are the statistical uncertainties. Prominent and distinct time structures visible in both the positron spectrum and the electron spectrum and at different energies are marked by dashed vertical lines.

To study the time behavior in more detail, the fluxes are shown in Fig. 2 as a function of time for five characteristic energy bins. We find a clear evolution of the fluxes with time at low energies that gradually diminishes towards high energies. At the lowest energies, the amplitudes of both the electron flux and the positron flux change by a factor of 3. Both fluxes exhibit profound short- and long-term variations. The short-term variations occur simultaneously in both fluxes with approximately the same relative amplitude.

On the short term of Bartels rotations, several prominent and distinct structures are observed. They are characterized by minima, visible in both the electron flux and the positron flux across the energy range below $E \lesssim 10$ GeV. These are marked by dashed vertical lines in Fig. 2. Variations on short timescales have been observed at different heliographic latitudes in the combined proton and antiproton flux and also in the combined electron and positron flux [40]. A possible origin has been discussed [41].

In October 2011 and March 2012, there are sharp drops in the fluxes, followed by a quick recovery. The March 2012 event coincides with a strong Forbush decrease registered on March 8, 2012 [42].

Another drop occurred in August 2012; this was followed by an extended recovery period.

For $E \lesssim 10$ GeV, May 2013 and April 2015 mark two changes in the long-term trends of the fluxes: From May 2011 to May 2013, the fluxes of both species show a trend to decrease with time. In the period around July 2013 is the time of the solar magnetic field reversal. From May 2013 to April 2015, the flux of electrons continues to decrease, but with reduced slope, while the positron flux begins to increase.

Then, from April 2015 until May 2017, both fluxes rise steeply. The difference of the rate of the increase is related to the charge-sign dependent solar modulation [15,43].

Coincident changes in both the short-term and long-term behavior have also been observed in our measurement of the proton and helium fluxes [18].

At energies above 20 GeV, neither the electron flux nor the positron flux exhibits significant time dependence.

The high statistics and continuous data presented in this Letter allow for the first time the detailed analysis of the time evolution of the spectral indices $\gamma_{e^{\pm}} = d(\log \Phi_{e^{\pm}})/d(\log E)$ [32]. They are displayed at a characteristic energy of 10 GeV in Fig. SM 4 [34]. We observe that the spectral indices for both the electrons and the positrons harden continuously with different slopes until April 2015 and then continue to soften with an identical slope. The prominent and distinct short-term structures discussed above are visible as a hardening in the spectral indices.

The long-term time structure of the data in Fig. 2 shows that the changes in relative amplitude are different for electrons and positrons. To quantify this effect, we use the ratio R_e, shown in Fig. 3. In Fig. SM 5 [34], we show our results on R_e for all energy bins up to 5 GeV.

In R_e, the important, newly discovered short-term variations in the fluxes largely cancel, and a clear overall long-term trend appears. At low energies, R_e is flat at first, then smoothly increases after the time of the solar magnetic field reversal, to reach a plateau at a higher amplitude.

During the extraordinarily quiet solar minimum period from 2006 to 2011, the energy and time dependence of various cosmic-ray measurements [44] including R_e
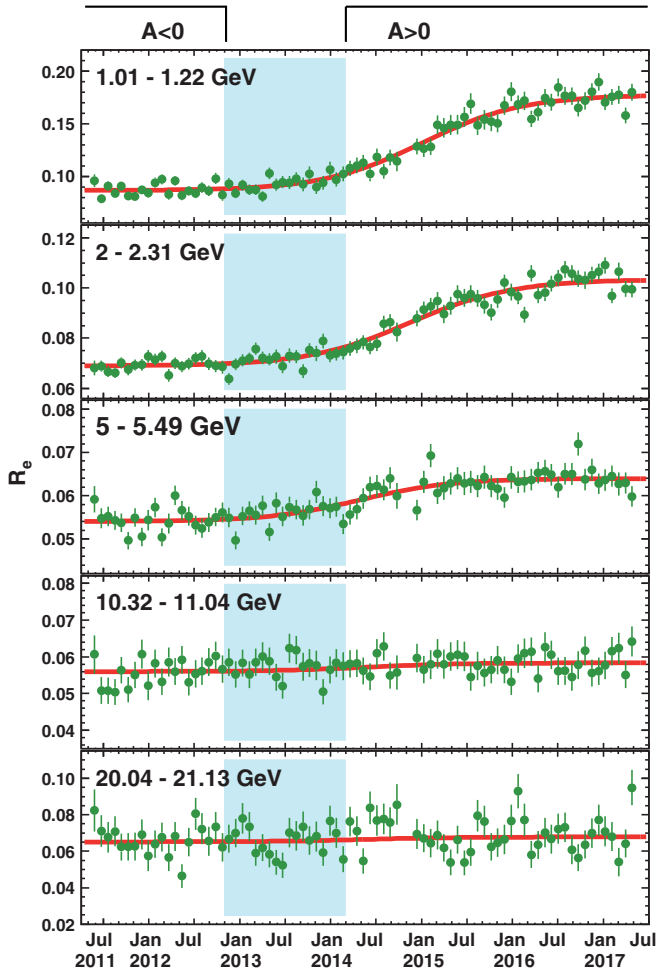
FIG. 3. The ratio R_e of the positron flux to the electron flux as a function of time. The error bars are statistical. The best-fit parametrization according to Eq. (3) is shown by red curves. The polarity of the heliospheric magnetic field is denoted by $A < 0$ and $A > 0$. The period without well-defined polarity is marked by the shaded area [17].
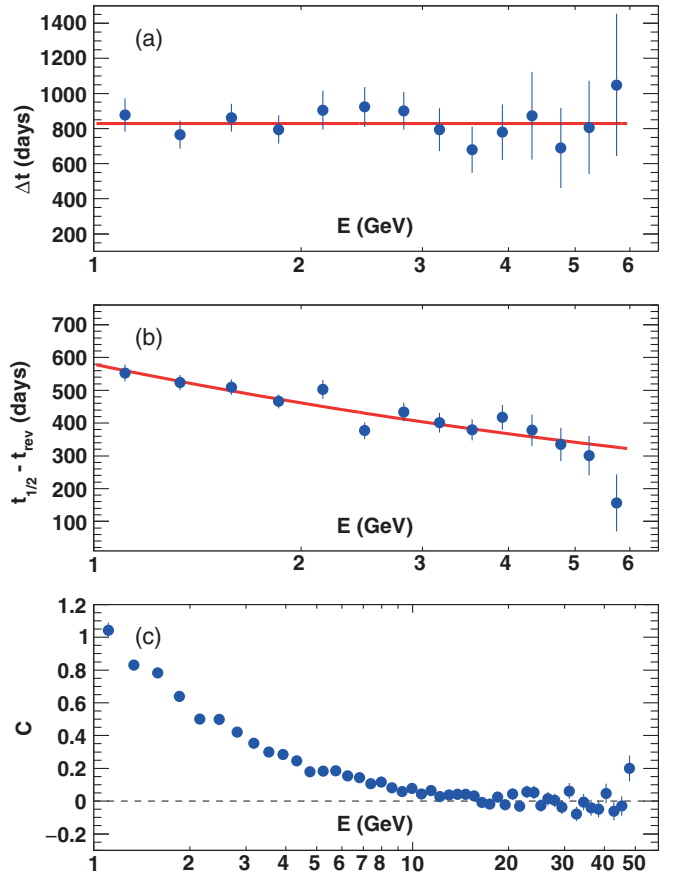

FIG. 4. Results of the fits of the parametrization in Eq. (3) to the ratio R_e as a function of energy (blue circles): (a) Δt and the best-fit constant value of 830 days (red line), (b) $t_{1/2} - t_{\rm rev}$ with the parametrization according to Eq. (4) (red curve), (c) amplitude C with a dashed line at zero to guide the eye.

At a given energy E, the time dependence is related to three parameters in the function: the amplitude of the transition C, the midpoint of the transition $t_{1/2}$, and the duration of the transition Δt. We choose $\Delta_{80} = 4.39$, such that Δt is the time it takes for the transition to proceed from 10% to 90% of the change in magnitude. The results of fitting Eq. (3) for each energy bin are shown in Fig. 4. We obtain $\chi^2/\text{d.o.f.} \approx 1$ for all fits.

The parameters $t_{1/2}$ and Δt can only be determined at low energies, where the amplitude of the transition is large, see Fig. 3. As shown in Fig. 4(a), the transition duration Δt is independent of energy, and we obtain a value of 830 ± 30 days.

Figure 4(b) shows the energy dependence of the delay $t_{1/2}$ which is well parametrized by the formula

$$t_{1/2}(E) - t_{\rm rev} = \tau (E/\text{GeV})^\rho, \qquad (4)$$

where we choose $t_{\rm rev}$ to be the effective time of the reversal of the solar magnetic field. For the value of $t_{\rm rev}$, we use July 1, 2013, the center of the period without well-defined polarity [17]. The parameters used to describe the time and

(Fig. SM 6 [34]) are well reproduced by advanced numerical solar modulation models [22]. But for the following years covered by the new data presented in this Letter, important and large systematic discrepancies are observed in particular in R_e (Fig. SM 6 [34]), which is sensitive to charge-sign dependent effects in the solar modulation process of galactic cosmic rays. Therefore, restricted to the time interval covered here, we use a model-independent approach to extract the energy dependence of the quantities that characterize the observed transition in R_e. With a set of four parameters, the 3871 independent R_e measurements as a function of energy and time can be described well with a logistic function,

$$R_e(t, E) = R_0(E) \left[1 + \frac{C(E)}{\exp\left(-\frac{t - t_{1/2}(E)}{\Delta t(E)/\Delta_{80}}\right) + 1} \right]. \qquad (3)$$

energy dependence of R_e in Eqs. (3) and (4) are illustrated in Fig. SM 7 [34]. A fit of Eq. (4) yields the parameter $\rho = -0.33 \pm 0.04(\text{stat})^{+0.08}_{-0.15}(\text{syst})$ and the amplitude $\tau = 580 \pm 19(\text{stat}) \pm 136(\text{syst})$ days, and the value of $t_{1/2}$ changes by 260 ± 30 days from 1 to 6 GeV. The systematic uncertainties are due to the uncertainty in t_{rev}. This is an important and unexpected energy dependence of $t_{1/2}$ and reflects the different response of cosmic-ray particles and antiparticles to changing modulation conditions.

To study the amplitude C in Fig. 4(c), we have fixed Δt to its average value of 830 days and we use the value of $t_{1/2}$ calculated from Eq. (4) for energies above 6 GeV. At high energies, the fit result for the amplitude depends only weakly on the choice of the values for Δt and $t_{1/2}$. As seen in Fig. 4(c), the amplitude C is close to 1 at $E = 1$ GeV and decreases smoothly with energy. This is in qualitative agreement with the expectation from solar modulation models including drift effects [41] and with the results from Refs. [13–16]. Above 20 GeV, the amplitude is consistent with zero.

In conclusion, for the first time, the charge-sign dependent modulation during solar maximum has been investigated in detail by leptons alone. We observe prominent, distinct, and coincident structures in both the positron flux and the electron flux on a time scale of months. These structures are not visible in the e^+/e^- flux ratio. We also observe the existence of a long-term feature in the e^+/e^- flux ratio, namely, a smooth transition from one value to another, after the polarity reversal of the solar magnetic field. The duration of the transition is measured to be 830 ± 30 days, independent of energy. The transition magnitude is decreasing as a function of energy, consistent with expectations from solar modulation models including drift effects. The midpoint of the transition relative to the polarity reversal of the solar magnetic field changes by 260 ± 30 days from 1 to 6 GeV. These high-statistics, precision data on positrons and electrons provide accurate input to the understanding of solar modulation.

[a]Also at ASI, I–00133 Roma, Italy.
[b]Also at ASI Space Science Data Center (SSDC), I–00133 Roma, Italy; Present address: University of Sassari, I–07100 Sassari, Italy.
[c]Also at Wuhan University, Wuhan, 430072, China.
[d]Also at Sun Yat–Sen University (SYSU), Guangzhou, 510275, China.
[e]Also at ASI Space Science Data Center (SSDC), I–00133 Roma, Italy.
[f]Also at ASI Space Science Data Center (SSDC), I–00133 Roma, Italy; Present address: INFN Sezione di Trieste, I–34149, Trieste, Italy.
[g]Also at Nankai University, Tianjin 300071, China.
[h]Also at Institute of Theoretial Physics, Chinese Academy of Sciences, Beijing, 100190, China.

[1] H. V. Cane, Space Sci. Rev. **93**, 55 (2000).
[2] M. S. Potgieter, J. A. Le Roux, L. F. Burlaga, and F. B. McDonald, Astrophys. J. **403**, 760 (1993).
[3] M. S. Potgieter, Living Rev. Solar Phys. **10**, 3 (2013).
[4] A. W. Strong and I. V. Moskalenko, Astrophys. J. **509**, 212 (1998).
[5] C. Evoli, D. Gaggero, A. Vittino, G. Di Bernardo, M. Di Mauro, A. Ligorini, P. Ullio, and D. Grasso, J. Cosmol. Astropart. Phys. 02 (2017) 015.
[6] D. Maurin, F. Donato, R. Taillet, and P. Salati, Astrophys. J. **555**, 585 (2001).
[7] A. Putze, L. Derome, and D. Maurin, Astron. Astrophys. **516**, A66 (2010).
[8] M. S. Potgieter, Adv. Space Res. **53**, 1415 (2014).
[9] W. R. Webber, J. C. Kish, and D. A. Schrier, *Proceedings of the 18th International Cosmic Ray Conference*, Vol. 3, Bangalore, India (Tata Institute, Mumbai, India, 1983).
[10] J. M. Clem, D. P. Clements, J. Esposito, P. Evenson, D. Huber, J. L'Heureux, P. Meyer, and C. Constantin, Astrophys. J. **464**, 507 (1996).
[11] K. Abe *et al.*, Phys. Lett. B **670**, 103 (2008).
[12] O. Adriani *et al.*, Phys. Rev. Lett. **116**, 241105 (2016).
[13] B. Heber *et al.*, J. Geophys. Res. **107**, 1274 (2002).
[14] S. E. S. Ferreira and M. S. Potgieter, Astrophys. J. **603**, 744 (2004).
[15] B. Heber, A. Kopp, J. Gieseler, R. Müller-Mellin, H. Fichtner, K. Scherer, M. S. Potgieter, and S. E. S. Ferreira, Astrophys. J. **699**, 1956 (2009).
[16] B. Heber, Space Sci. Rev. **176**, 265 (2013).
[17] X. Sun, J. T. Hoeksema, Y. Liu, and J. Zhao, Astrophys. J. **798**, 114 (2015).
[18] M. Aguilar *et al.* (AMS Collaboration), preceding Letter, Phys. Rev. Lett. **121**, 051101 (2018).
[19] For example, I. Cholis and D. Hooper, Phys. Rev. D **88**, 023013 (2013).
[20] There are many models for the origin and propagation of cosmic rays. An overview and further references are given, e.g., in a recent review by R. Cowsik, Annu. Rev. Nucl. Part. Sci. **66**, 297 (2016).
[21] M. Cirelli, D. Gaggero, G. Giesen, M. Taoso, and A. Urbano, J. Cosmol. Astropart. Phys. 12 (2014) 045.
[22] N. Tomassetti, M. Orcinha, F. Barao, and B. Bertucci, Astrophys. J. Lett. **849**, L32 (2017).
[23] V. Di Felice, R. Munini, E. E. Vos, and M. S. Potgieter, Astrophys. J. **834**, 89 (2017).
[24] M. S. Potgieter and E. E. Vos, Astron. Astrophys. **601**, A23 (2017).
[25] R. Manuel, S. E. S. Ferreira, and M. S. Potgieter, Sol. Phys. **289**, 2207 (2014).
[26] L. Accardo *et al.*, Phys. Rev. Lett. **113**, 121101 (2014).
[27] A. W. Strong, I. V. Moskalenko, and V. S. Ptuskin, Annu. Rev. Nucl. Part. Sci. **57**, 285 (2007).
[28] M. Jubelgas, V. Springel, T. Enßlin, and C. Pfrommer, Astron. Astrophys. **481**, 33 (2008).
[29] M. Zhang, P. Zuo, and N. Pogorelov, Astrophys. J. **790**, 5 (2014).
[30] A. Kounine, Int. J. Mod. Phys. E **21**, 1230005 (2012); S. Rosier-Lees, *Proceedings of Astroparticle Physics TEVPA/ IDM*, Amsterdam, 2014 (unpublished); S. Ting, Nucl. Phys. B,

Proc. Suppl. **243–244**, 12 (2013); S.-C. Lee, *Proceedings of the 20th International Conference on Supersymmetry and Unification of Fundamental Interactions* (SUSY 2012), Beijing, 2012 (unpublished); M. Aguilar, *Proceedings of the XL International Meeting on Fundamental Physics, Centro de Ciencias de Benasque Pedro Pascual*, 2012 (unpublished); S. Schael, *Proceedings of the 10th Symposium on Sources and Detection of Dark Matter and Dark Energy in the Universe*, Los Angeles, 2012 (unpublished); B. Bertucci, Proc. Sci., EPS-HEP (**2011**) 67; M. Incagli, AIP Conf. Proc. **1223**, 43 (2010); R. Battiston, Nucl. Instrum. Methods Phys. Res., Sect. A **588**, 227 (2008).
[31] J. Allison *et al.*, IEEE Trans. Nucl. Sci. **53**, 270 (2006); S. Agostinelli *et al.*, Nucl. Instrum. Methods Phys. Res., Sect. A **506**, 250 (2003).
[32] M. Aguilar *et al.*, Phys. Rev. Lett. **113**, 121102 (2014).
[33] At low energies, multiple scattering distorts the particle trajectory extrapolated from the tracker into the TRD. We improve the reconstruction of the trajectory by incorporating the coordinate measurements from the TRD. This increases the effective acceptance by 40% at 1 GeV, and by 10% at 5 GeV. Above 8 GeV the improvement is negligible. N. Zimmermann, Ph.D. thesis, RWTH Aachen University (to be published); See also M. Graziani, Ph.D. thesis, Università degli Studi di Perugia (2015), https://cds.cern.ch/record/ 2278596.
[34] See Supplemental Material at http://link.aps.org/ supplemental/10.1103/PhysRevLett.121.051102 for additional figures and for the tabulated results on the electron flux, the positron flux, and the ratio R_e as functions of energy at the top of AMS time-averaged from May 2011 to May 2017 and for each Bartels rotation. Data for Bartels rotations 2472 and 2473 are absent because this period was devoted to detector studies. The data can also be downloaded in different formats from the ASI cosmic-ray database at https://tools.asdc.asi.it/CosmicRays/.
[35] G. D. Lafferty and T. R. Wyatt, Nucl. Instrum. Methods Phys. Res., Sect. A **355**, 541 (1995). We have used Eq. (6) with $\tilde{E} \equiv x_{lw}$.
[36] L. Ali Cavasonza, H. Gast, M. Krämer, M. Pellen, and S. Schael, Astrophys. J. **839**, 36 (2017). The model is defined in Eq. (2a) for the positron flux and Eq. (2b) for the electron flux.
[37] C. Corti, V. Bindi, C. Consolandi, and K. Whitman, Astrophys. J. **829**, 8 (2016). The prescription from Eq. (3) has been used to add a second smooth break at low energy for the electron flux in Eq. (2b) of Ref. [36].
[38] A. W. Strong, E. Orlando, and T. R. Jaffe, Astron. Astrophys. **534**, A54 (2011).
[39] M. S. Potgieter, E. E. Vos, R. Munini, M. Boezio, and V. Di Felice, Astrophys. J. **810**, 141 (2015).
[40] B. Heber, J. B. Blake, C. Paizis, V. Bothmer, H. Kunow, G. Wibberenz, R. A. Burger, and M. S. Potgieter, AIP Conf. Proc. **528**, 357 (2000).
[41] M. S. Potgieter, Adv. Space Res. **13**, 239 (1993).
[42] A. Cheminet, G. Hubert, V. Lacoste, D. Maurin, and L. Derome, J. Geophys. Res. Space Phys. **118**, 7488 (2013).
[43] M. S. Potgieter, R. A. Burger, and S. E. S. Ferreira, Space Sci. Rev. **97**, 295 (2001).
[44] M. S. Potgieter, Adv. Space Res. **60**, 848 (2017).